Available online at www.sciencedirect.com

SciVerse ScienceDirect

Ceramics International 38 (2012) 1497–1505

CERAMICS INTERNATIONAL

www.elsevier.com/locate/ceramint

Slag attack evaluation of in situ spinel-containing refractory castables via experimental tests and thermodynamic simulations

A.P. Luz [a,*], M.A.L. Braulio [a], A.G. Tomba Martinez [b], V.C. Pandolfelli [a]

[a] Federal University of São Carlos, Materials Engineering Department, Rod. Washington Luiz, km 235, São Carlos, SP 13565-905, Brazil
[b] Materials Science and Technology Research Institute (INTEMA), Ceramics Division, Av. Juan B. Justo 4302, 7600 Mar del Plata, Argentina

Received 8 September 2011; accepted 14 September 2011
Available online 19 September 2011

Abstract

Although the in situ spinel formation in alumina–magnesia refractory castables induces an expansive behavior, many investigations highlight its positive role in the corrosion resistance of such materials. Thus, this work addresses the slag attack evaluation of four designed in situ spinel-containing castables (containing hydratable alumina or calcium aluminate cement as a binder source and 0 or 1 wt% of silica fume) when in contact with a Fe_xO rich industrial slag. Corrosion cup-tests, microstructural characterization and a two-step thermodynamic simulation model were used in order to investigate the reactions taking place during the slag–refractory interactions. According to the attained results, hydratable alumina seems to be a suitable binder to improve the corrosion resistance of such castables, as it induces densification and the formation of an alumina-rich spinel phase at the slag–matrix interface. Moreover, the thermodynamic calculations matched to the experimental observations, attesting the efficiency of the proposed simulation model for the evaluation of the in situ spinel-containing castable corrosion behavior.

Keywords: C. Corrosion; Spinel-containing castables; Slag; Thermodynamic simulation

1. Introduction

Spinel ($MgAl_2O_4$) containing castables are widely used in steel ladles due to their outstanding thermo-mechanical properties, extended service life and chemical resistance [1]. Many investigations highlighted that fine and well distributed $MgAl_2O_4$ grains, formed in situ by the reaction of MgO and Al_2O_3 in the castable matrix, can increase slag corrosion resistance when compared to pre-formed spinel containing ones [2–5]. According to the proposed mechanism [2,4], CaO from the slag reacts with Al_2O_3 (available in the castable composition) forming calcium aluminate phases (CA_2 and CA_6), whereas Mn^{2+}, Fe^{2+} and Fe^{3+} ions can be trapped into the spinel structure via solid solutions. As a consequence, the slag becomes silica-rich, leading to a more viscous liquid and inhibits its penetration into the castable porosity. However, the in situ spinel generation is followed by a volumetric expansion and an exceeded reaction can lead to microcracking, giving rise to novel paths for further slag infiltration.

Some parameters (such as the MgO and alumina grain sizes [6,7], the binder system [8–10], the silica fume content [11–13] and the refractory aggregate sources [14]) influence the volumetric stability of the alumina–magnesia castables. The binder system can affect the in situ spinel formation and its expansive behavior due to its reactions and sinterability at high temperatures. Some authors [6] stated that the use of calcium aluminate cement (CAC) may lead to further expansion, which is mainly associated to CA_2 and CA_6 formation (where $C = CaO$ and $A = Al_2O_3$). Conversely, hydratable alumina (which is a binder based on the re-hydration ability of ρ-Al_2O_3) is an alternative material that can inhibit the CA_6 formation (due to the lack of CaO), resulting in a less porous microstructure containing finer spinel grains [6,7].

Regarding the silica fume role in the Al_2O_3–MgO castables properties, its addition to cement containing compositions can induce the presence of low melting temperature phases and a counterbalancing effect on the spinel disruptive expansion [11]. Moreover, this additive affects the calcium aluminates (CA_2 and CA_6) generation and speeds up $MgAl_2O_4$ formation, due to the ion diffusion increase in the presence of liquid phases [12,13]. Despite these advantages, high liquid contents result in

* Corresponding author. Tel.: +55 16 33518253; fax: +55 16 33615404.
E-mail address: anapaula.light@gmail.com (A.P. Luz).

0272-8842/$36.00
doi:10.1016/j.ceramint.2011.09.033

shrinkage and decrease the castables refractoriness and corrosion resistance [14]. Conversely, the presence of silica fume in hydratable alumina bonded castables can also lead to a lower amount of a metastable SiO_2–Al_2O_3 liquid phase formation (~1250 °C), providing densification and reducing the overall in situ spinel expansion.

Based on these aspects, this work investigates the corrosion behavior of four designed alumina–magnesia castable compositions (containing hydratable alumina or calcium aluminate cement as a binder source and 0 or 1 wt% of silica fume) when in contact with high-iron oxide containing industrial slag at 1500 °C. Corrosion cup-tests, microstructural characterization (SEM–EDS) and thermodynamic calculations were carried out in order to evaluate and understand the possible reactions taking place during the slag–refractory interaction. An optimized thermodynamic simulation procedure [15] (where firstly the molten slag was placed in contact with the matrix components and later with the aggregates) was applied and the calculated results were presented, discussed and compared with the experimental ones.

2. Experimental and thermodynamic calculations

Four vibratable alumina–magnesia castables were designed according to the Alfred particle packing model ($q = 0.26$) [16]. The compositions comprised coarse tabular alumina as aggregates ($d \leq 6$ mm, Almatis, USA), dead-burnt magnesia ($d < 45$ μm, 95 wt% of MgO, $CaO/SiO_2 = 0.37$, Magnesita Refratários S.A., Brazil), reactive alumina (CL370, Almatis, USA), fine tabular alumina ($d < 200$ μm, Almatis, USA), silica fume (971U, Elkem, Norway) and calcium aluminate cement (CAC, Secar 71, Kerneos, France) or hydratable alumina (HA, AlphaBond 300, Almatis, USA) as binders. Table 1 presents the overall compositions evaluated in this work. A total of 6 wt% of MgO was added to the designed castables in order to result in 21 wt% of stoichiometric in situ spinel (72 wt% Al_2O_3–28 wt% MgO) after the reaction with calcined and fine tabular Al_2O_3 particles during the pre-firing step at 1500 °C.

The castable dispersion was carried out by adding 0.2 wt% of a polycarboxylate based dispersant (Bayer, Germany), leading to 3.9–4.1 wt% (CAC) or 5.3 wt% (HA) water content for a suitable vibratable shaping. After the mixing step, cylindrical samples with an external diameter of 10 cm, 10 cm in height, a central inner hole 5 cm in diameter and 5 cm deep were molded, cured at 50 °C for 24 h [in a humid environment (relative humidity = 100% for castables containing CAC – AM-6CAC0S and AM-6CAC1S) and at room conditions (relative humidity = 40% for the ones bonded with hydratable alumina – AM-6HA0S and AM-6HA1S)], dried at 110 °C for 24 h, calcined at 600 °C for 5 h and thermally treated at 1500 °C for 5 h (this last step was required in order to allow the in situ spinel and CA_6 formation).

Before the corrosion tests, the cup samples were filled in with 150 g of an industrial slag (Table 2). The corrosion cup tests were conducted in an electrical furnace (Lindberg Blue, Lindberg Corporation, USA) in an oxidizing atmosphere (oxygen partial pressure = 0.21 atm) at 1500 °C for 2 h.

After that, the corroded samples were cut and had their cross sections polished and prepared for scanning electron microscopy analysis (JEOL, JSM-7500F model, Germany). In addition, the slag penetration area was calculated using the Image J 1.42q software (Wayne Rasband, National Institutes of Health, USA), according to the procedure described by Braulio et al. [5] in order to quantify the corrosion damage.

Thermodynamic simulations were carried out using FactSage™ version 6.2 [Thermfact/CRCT (Montreal) and GTT-Technologies (Aachen)]. Fact53, SGTE, FToxid databases and the Equilib and Viscosity modules were selected for this evaluation. All calculations were conducted considering a constant temperature of 1500 °C and pressure of 1 atm. Based on a two-step modeling calculation (previously developed by the authors [15]), initially 100 g of slag and 100 g of the castable matrix (Table 3) were reacted and the resulting liquid after each step was successively placed in contact with the original matrix, until the slag saturation was reached.

After that, 100 g of the resulting slag (liquid saturated with the matrix components) was used in the calculations involving 100 g of the aggregates. Due to the in situ $MgAl_2O_4$ and CA_6 formation (the latter taking place only for the CAC containing compositions) at the pre-firing step at 1500 °C, these formed phases were also considered for the matrix simulation (Table 3). In order to define the matrix composition for the thermodynamic simulations, not only the amount of the initial raw materials of the designed castables was considered, but also the results attained by quantitative X ray diffraction (XRD) and scanning electron microscopy (SEM–EDS) evaluations of the fired samples [5] were used.

3. Results and discussion

3.1. Corrosion cup-tests and microstructural analysis

Fig. 1 presents the corroded sample images and the calculated penetration area after the slag infiltration. The

Table 1
General information related to the castable compositions.

Raw materials (wt%)	AM-6CAC0S	AM-6CAC1S	AM-6HA0S	AM-6HA1S
Tabular and calcined alumina	88	87	88	87
Dead-burnt magnesia	6	6	6	6
Calcium aluminate cement	6	6	–	–
Hydratable alumina	–	–	6	6
Silica fume	–	1	–	1

AM: alumina magnesia; CAC: calcium aluminate cement; S: silica fume.

Table 2
Chemical composition of the industrial slag used in this work.

Components	Fe_2O_3	CaO	SiO_2	MgO	MnO	Al_2O_3	P_2O_5	TiO_2	Cr_2O_3	SO_3	CaO/SiO_2
Wt%	40.8	34.2	8.7	8.5	4.1	1.6	1.4	0.4	0.2	0.1	3.9

Table 3
Matrix and aggregates compositions considered for the thermodynamic simulations.

Components (wt%)	Matrix ($d < 100$ μm)				Aggregates ($d > 100$ μm)			
	AM-6CAC0S	AM-6CAC1S	AM-6HA0S	AM-6HA1S	AM-6CAC0S	AM-6CAC1S	AM-6HA0S	AM-6HA1S
Al_2O_3	15.8	12.8	43.0	41.6	78.8	89.4	100.0	100.0
CaO	1.0	1.8	–	–	–	–	–	–
CA_6	10.3	20.5	–	–	21.2	10.6	–	–
$MgAl_2O_4$	72.9	62.0	57.0	55.8	–	–	–	–
SiO_2	–	2.9	–	2.6	–	–	–	–

hydratable alumina containing compositions (AM-6HA0S and AM-6HA1S) showed the highest corrosion resistance at the tested conditions.

Despite the silica fume advantages (i.e., increasing the flowability and improving the MgO hydration resistance due to magnesium–silicate–hydrate formation during the castable processing step [9,17], etc.), its addition to the alumina–magnesia composition containing calcium aluminate cement (AM-6CAC1S) reduced the corrosion resistance and induced a relative increase in the slag infiltration of about 58%, when compared to the AM-6CAC0S castable (Fig. 1). The same trend was not observed for the hydratable alumina bonded materials and, due to the absence of CaO, a lower amount of a viscous Al_2O_3–SiO_2 based liquid phase was formed, leading to sintering, densification and, consequently, a better corrosion performance for the AM-6HA1S castable.

In addition, according to the CaO–Al_2O_3–SiO_2–MgO system [17], the AM-6CAC1S matrix composition should be located in the $MgAl_2O_4$–CA_6–$Ca_2Al_2Si_2O_8$–$Ca_2Al_2SiO_7$ compatibility tetrahedron and a liquid phase would be present above 1350 °C. Therefore, when exposed at high temperatures (>1350 °C) and in contact with molten slag, it is expected that this liquid phase formed in the AM-6CAC1S castable might be incorporated by the slag, resulting in further infiltration and reaction with the solid refractory.

Previous investigations carried out by the authors [5] showed that the spinel phase was detected in the matrix region of the cement containing pre-fired samples (before the corrosion tests), but depending on the CaO reaction mechanism for the CA_6 formation (solid state or precipitation from the liquid for silica free or silica containing composition, respectively), some changes in the location of the calcium hexaluminate grains was observed. The AM-6CAC0S castable, for instance, contained CA_6 equiaxial grains at the edges of the tabular alumina aggregates, whereas the AM-6CAC1S ones presented needle-like crystals dispersed in the matrix region. The calcium hexaluminate phase formed at the tabular alumina surface has a high melting point (~1830 °C) and leads to densification [11–13], which is responsible for the lower slag penetration area attained for the AM-6CAC0S when compared with AM-6CAC1S samples.

Nevertheless, some authors [18–21] also suggested that the corrosion resistance of this sort of refractory can be spoiled due to the stress built up between Al_2O_3 and CA_6, which can result

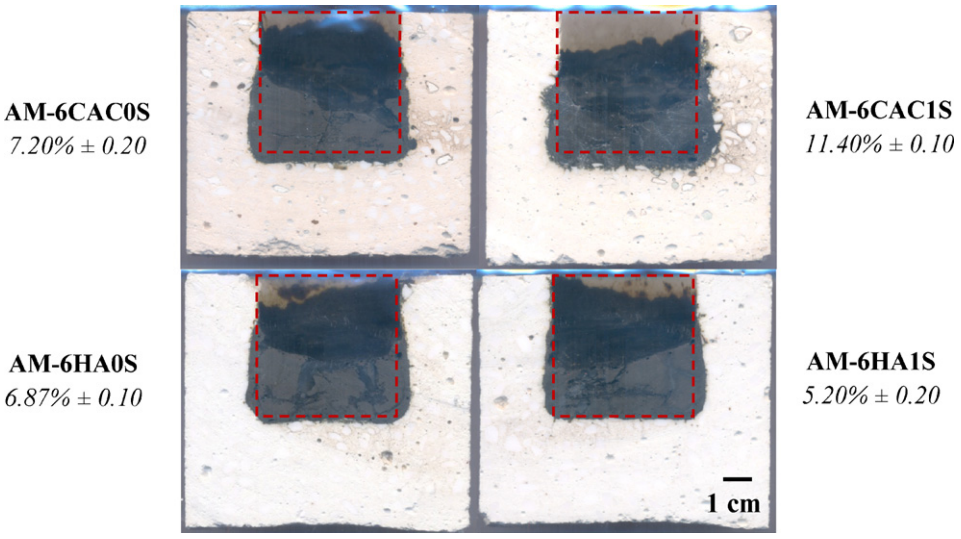

Fig. 1. Cross sections and penetration area (%) of the corroded samples. The dotted area indicates the original inner cup dimension.

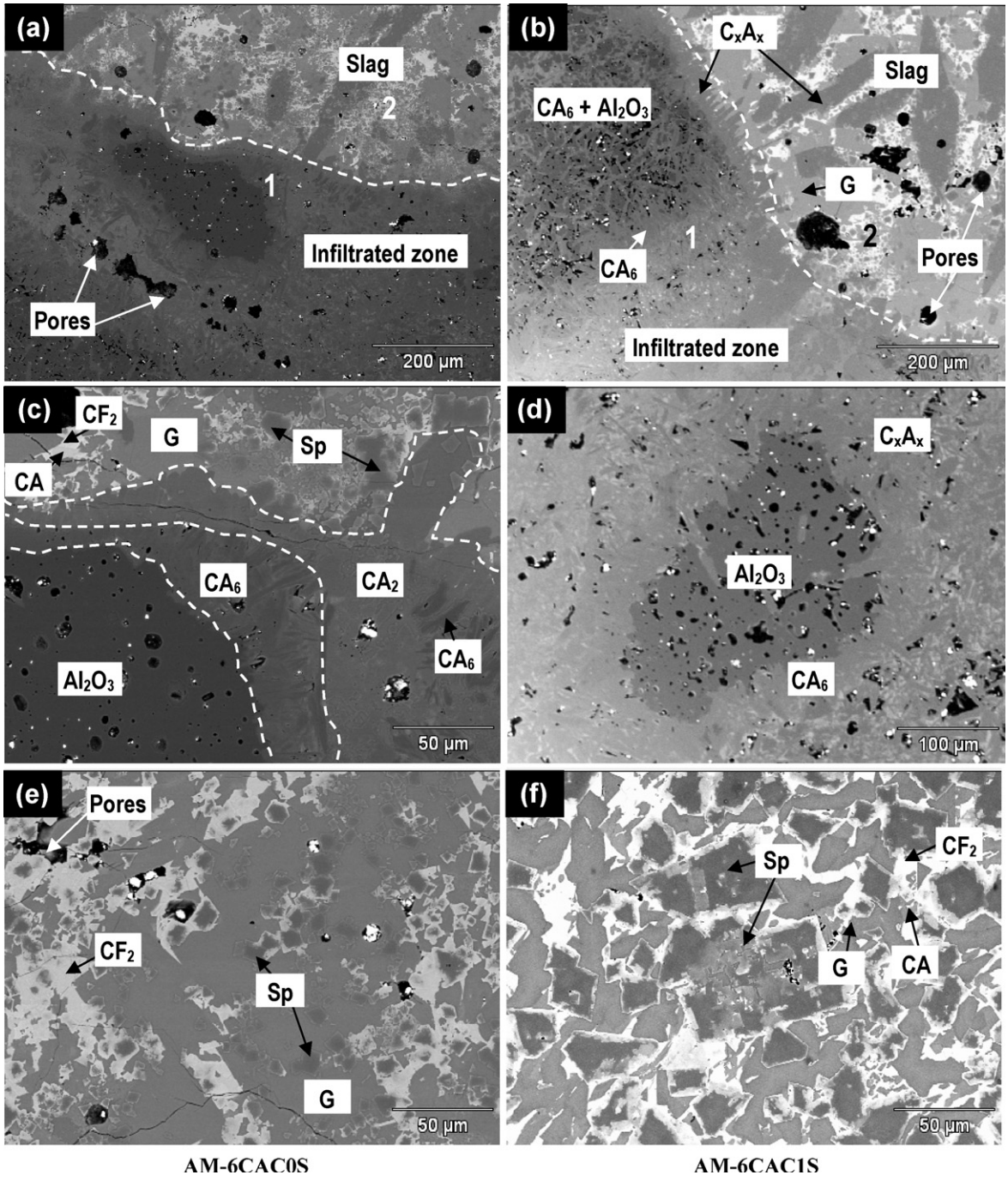

Fig. 2. Corroded region and remaining slag after the corrosion cup-tests of the CAC bonded castable samples: AM-6CAC0S (a, c, and e) and AM-6CAC1S (b, d, and f). Micrographs (c) and (d) present (with a higher magnification) the slag–castable interface area identified as 1 in (a) and (b), whereas the slag zone (indicated by 2) is shown in (e) and (f). G: gehlenite (C_2AS); C_xA_x: $CA_6 + CA_2$ containing Fe_2O_3; Sp: spinel solid solution ($MgAl_2O_4 + MgFe_2O_4$ containing MnO).

in the interface disintegration allowing the molten slag to penetrate, most likely through the Al_2O_3 grain boundaries, into the bulk specimen. The presence of microcracks in the CAC bonded castable samples (after the pre-firing treatment at 1500 °C) was not detected by the SEM analyses, but the following apparent porosity values were attained: AM-6CAC0S = 20.99 ± 0.41%, AM-6CAC1S = 23.08 ± 0.36%, AM-6HA0S = 21.19 ± 1.07% and AM-6HA1S = 19.33 ± 0.17%. Thus, the higher slag penetration presented by the AM-6CAC1S samples might be also related to the higher porosity of this castable.

Regarding the hydratable alumina bonded compositions, a less porous microstructure and finer alumina-rich spinel grains were detected in the samples matrix [5]. The ability of spinel to incorporate Fe^{2+}, Fe^{3+}, Mg^{2+} and Mn^{2+} into Mg^{2+} vacancies (when in contact with molten slags) is pointed out as the main mechanism responsible for the lower slag penetration of these samples [21].

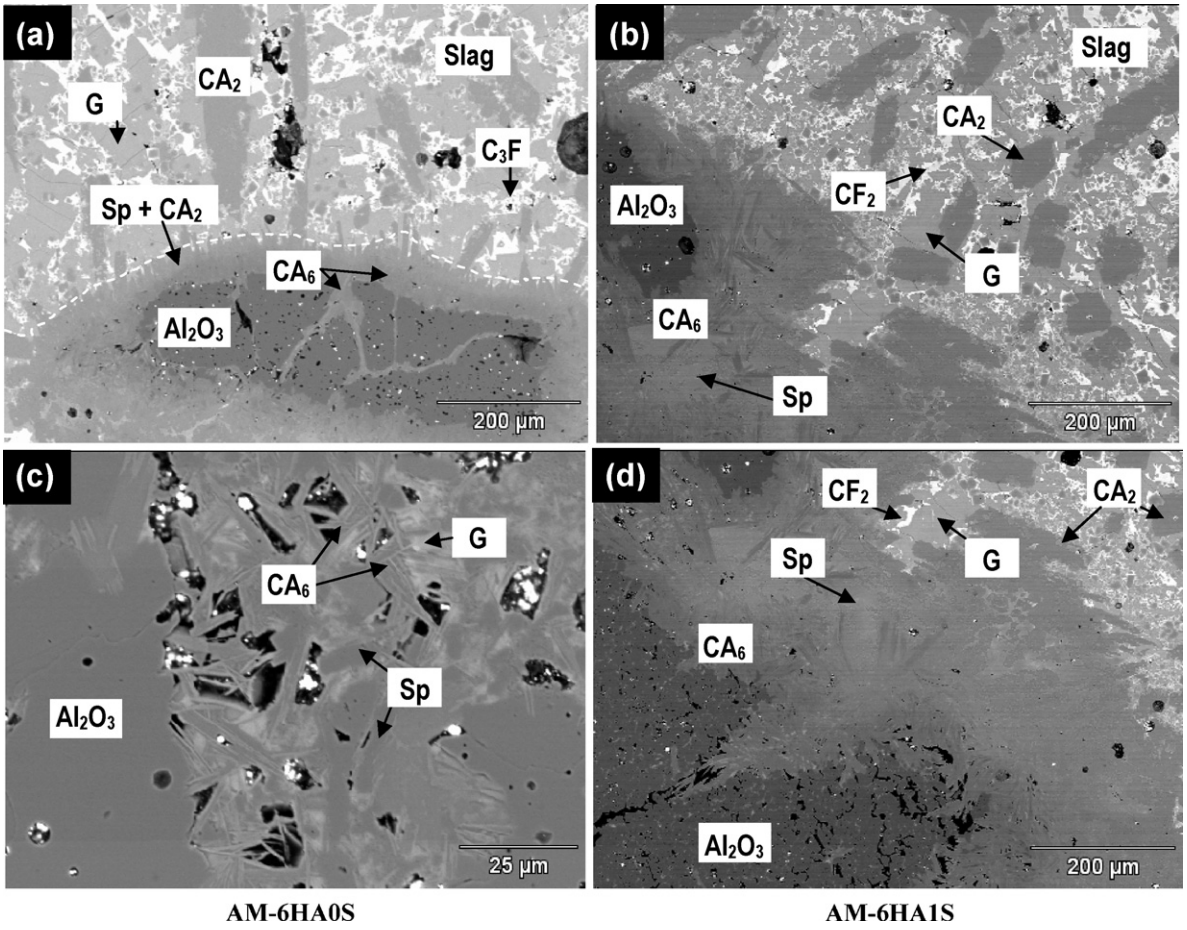

Fig. 3. Corroded region of the hydratable alumina bonded castable samples: AM-6HA0S (a and c) and AM-6HA1S (b and d). G: gehlenite (C_2AS); Sp: alumina rich spinel (containing iron and manganese in its composition).

Figs. 2 and 3 present the microstructural analysis of the corroded samples. The CAC bonded castables showed calcium aluminate phases (presenting some iron content into their compositions) formed at the edge of the tabular alumina aggregates and all $MgAl_2O_{4(ss)}$ grains previously located at the slag–castable matrix interface were readily dissolved by the liquid (Fig. 2a–d). The corroded AM-6CAC1S samples did not show well defined CA_6 and CA_2 layers and a mixture of these phases (C_xA_x) was identified in the infiltrated zone and slag area. In addition, the high Al_2O_3 content available close to the aggregates surface led to the formation of a higher amount of CA_6 grains in this area, resulting in volumetric expansion [2,5] and, consequently, in the tabular alumina coarse grains fragmentation (Fig. 2b).

Conversely, the presence of these calcium aluminate phases in the AM-6CAC0S microstructure seems to protect the alumina particles and inhibit the advance of the slag attack (Fig. 2a and c). The CA_2 layer was more compact and finer than the CA_6 one. Furthermore, CA_2 was not only detected in this layer, but also at the slag interface as large grains.

Spinel phase (solid solution containing approximately 69 wt% of alumina, 7–15 wt% of iron and 1–3 wt% of manganese) was detected in the remaining slag area displaying a cubic morphology (indicating their precipitation from the liquid) and average particle sizes of about 10 μm and 30 μm for AM-6CAC0S and AM-6CAC1S samples, respectively (Fig. 2e and f). According to the EDS analysis, CA, CF_2 or a glassy phase containing iron and a mixture of CaO, Al_2O_3 and SiO_2 that could be gehlenite, were also identified in the corroded samples of the CAC bonded compositions.

For the castable samples comprising hydratable alumina as the binder system, the same phase transformations described above were observed (Fig. 3). However, besides the finer $MgAl_2O_{4(ss)}$ grains precipitated in the remaining slag, a mixture of CA_2 large grains and alumina rich spinel phase (containing 78 wt% of alumina, 8–10% of iron and 1–3 wt% of manganese) layer was also observed closer to the slag–refractory interface.

Due to the compact aspect of this alumina rich spinel phase, its morphology could not be defined. The presence of this phase at the corroded interface of the AM-6HA0S and AM-6HA1S refractories might be an indicative that a portion of the original spinel crystals, formed during the pre-firing step at the samples matrix, was not completely attacked by the slag. Additionally, the spinel phase at the slag–refractory interface can also act as a nucleus for the growth of further grains (enriched in manganese and iron) into the slag [2,4], improving the corrosion resistance of such materials by the consumption of the deleterious ions from the liquid.

Nevertheless, the higher mobility of the Ca^{2+} ions contained in the molten slag allowed the formation of calcium

hexaluminate grains close to the alumina aggregates (Fig. 3). CA_6 grains were formed in the presence of spinel, gehlenite and glassy phases, as highlighted in Fig. 3c.

3.2. Thermodynamic calculations

According to the proposed model, a two-step simulation was carried out for the slag–matrix (step A) and slag–aggregates (step B) interactions at 1500 °C, and the collected results are presented as follows.

3.2.1. Slag–matrix interaction (step A)

The phase evolution predicted for the castable' matrix and molten slag contact are presented in Fig. 4. Due to the chemical differences between the designed refractories and the initial slag composition, dissolution and interdiffusion of various components are carried out, resulting in a compositional gradient which can lead to $MgAl_2O_{4(ss)}$, CA_2 and/or CA_6 formation. Moreover, with the slag–castable reaction progress, the liquid composition changes and as it becomes saturated by the refractory components, no further attack takes place.

The last calculation step, shown at the right corner of each graph in Fig. 4, presents the fired castable compositions attained by thermodynamic simulations, disregarding mullite, liquid and minor phases. These values were used to define at which step the successive calculation procedure could be interrupted. Thus, based on the number of calculation steps required to attain a saturated slag, it can be determined which refractory composition would have the highest corrosion resistance.

Castable AM-6HA1S, for instance, required only 8 calculation steps in order to reach the liquid saturation. On the other hand, a total of 23 steps were carried out for the AM-6CAC1S, pointing out that this refractory matrix is more reactive and prone to be attacked by the molten slag. Hence, the following corrosion resistance ranking can be predicted: AM-6HA1S (8 steps) > AM-6HA0S (10 steps) > AM-6CAC0S (12 steps) > AM-6CAC1S (23 steps). These results are in agreement with the experimental data presented in Fig. 1.

As expected, a higher liquid content was attained for the silica fume containing castables (Fig. 4b and d) for both evaluated binders, indicating that a greater amount of the refractory (solid and liquid phases) is dissolved and incorporated into the slag. In addition, a drop in the liquid amount after the 4th and 2nd steps for AM-6CAC1S and AM-6HA1S, respectively, is related to the spinel, CA_2 and/or CA_6 precipitation. Due to the absence of CaO in the AM-6HA1S composition, the only source for this oxide might have been the slag. Therefore, the CA_6 formation is induced by the higher supply of Al_2O_3 in the matrix of this castable and, as observed in the experimental results (Fig. 3), the calcium hexaluminate phase was located close to the aggregates particles. The corundum phase was also detected in an earlier step of the simulation results, indicating that AM-6HA1S refractory should have the highest corrosion resistance, as the thermodynamic equilibrium would have been attained. Moreover, CA_2

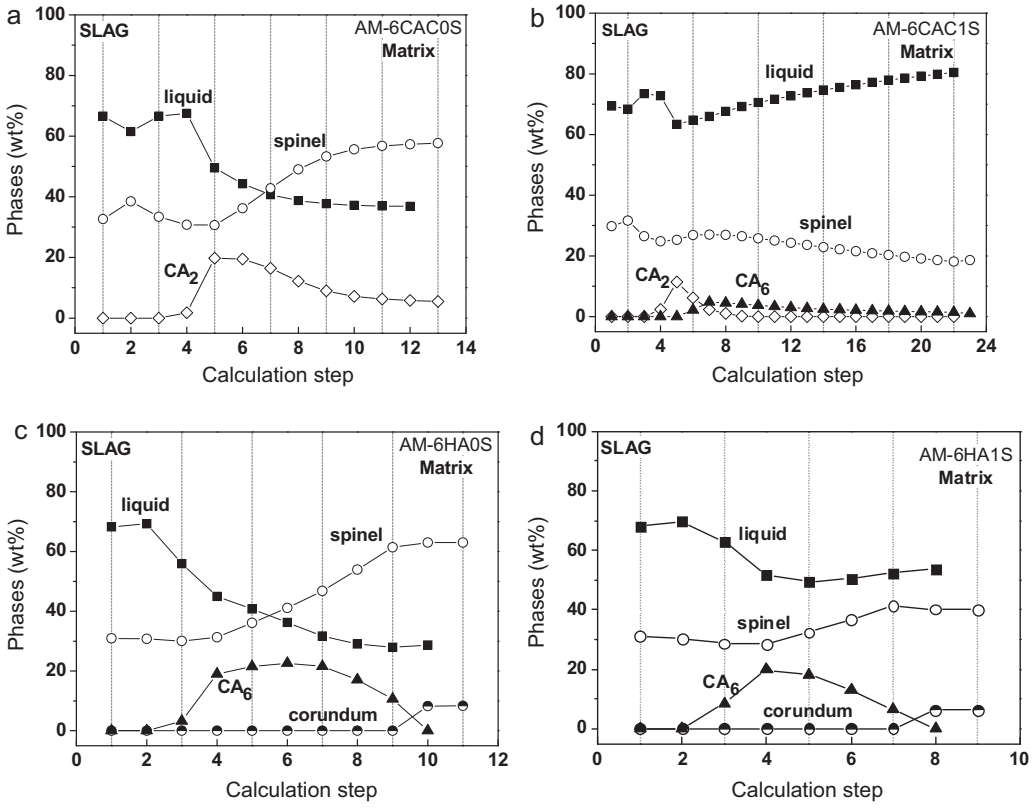

Fig. 4. Phase evolution predicted by the thermodynamic simulations for the contact involving slag–matrix compositions: (a) AM-6CAC0S, (b) AM-6CAC1S, (c) AM-6HA0S and (d) AM-6HA1S.

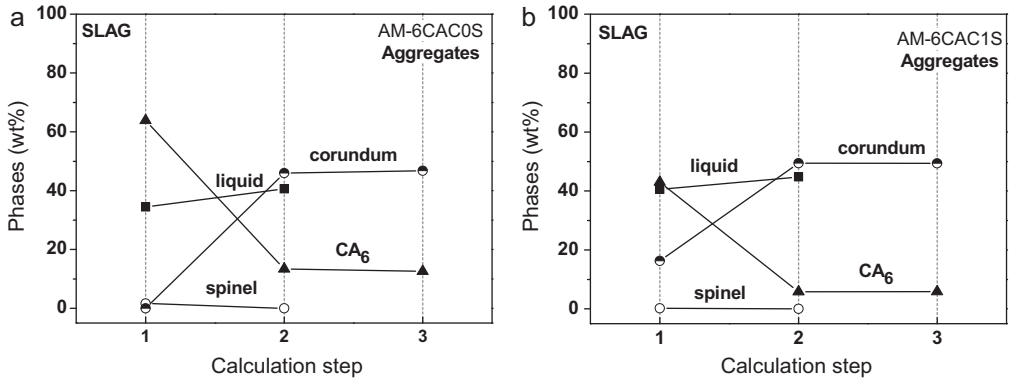

Fig. 5. Phase evolution predicted by the thermodynamic simulations for the interaction slag–aggregate: (a) AM-6CAC0S and (b) AM-6CAC1S.

precipitation was not predicted by the thermodynamic calculations for the slag–AM-6HA1S matrix interaction. Therefore, the identified grains of the dicalcium aluminate phase shown in the slag area of Fig. 3b might have been formed during the samples' cooling step or under a non-equilibrium state.

When silica fume was not added to the refractory compositions some important changes were observed and $MgAl_2O_{4(ss)}$ turned out to be the main crystalline phase of the system, presenting higher amounts than the liquid one, after some calculation steps. Despite the high liquid content (60–70 wt%) attained after the first slag–silica free matrix (AM-6CAC0S and AM-6HA0S) interaction, this molten phase is readily consumed and spinel and CA_2/CA_6 are precipitated from the liquid (Fig. 4). The precipitated spinel should contain FeO/Fe_2O_3 and MnO into the solid solution, and, for this reason, its content and composition can change with the advance of the refractory wearing. Moreover, this effect is not only observed for the spinel, but also for the calcium aluminates (CA_2 and CA_6 which can incorporate mainly iron into their solid solutions, as predicted by the calculations) and the corundum (which contains iron and manganese in its composition [15]). Another important aspect to be highlighted is the limited amount of Al_2O_3 in the IS-6CAC0S matrix, which most likely is the main reason for the CA_2 generation instead of CA_6 phase, as presented in Fig. 4a.

3.2.2. Slag–aggregates interaction (step B)

Because the resulting liquid from the slag–hydratable alumina bonded matrix simulation was saturated with alumina, no reactions between slag and tabular alumina aggregates were detected and, therefore, the thermodynamic results of this evaluation are not presented in Fig. 5. In addition, CA_2 and CA_6 formation is limited due to the lower alumina content in the CAC bonded matrix (Fig. 3a and b), nevertheless the interaction of the resulting slag with the tabular alumina aggregates led to CA_6 generation (Fig. 5, step 1). This aspect indicates that the CA_6 equiaxial grains formed at the edges of the aggregates of the AM-6CAC0S samples [5] during the pre-firing step and the CA_2 layer derived from the slag–matrix interaction can protect the refractory and inhibit further slag attack.

However, calcium hexaluminate formation is followed by a volumetric expansion ($\Delta V = 3.01\%$ [2,5,15]) and a great amount of this phase at the slag–aggregates interface might result in a continuous liquid penetration and reaction with the refractory sample.

Based on the total amount of CA_2 and CA_6 predicted to be formed during the corrosion process of the in situ spinel-containing compositions evaluated in this work (Table 4), it is clear that calcium hexaluminate formation is restricted to the matrix region for the hydratable alumina containing castables and that the best corrosion resistance performance of the AM-6HA1S refractory (Fig. 1) is also related to its lower content. On the other hand, the total amount of CA_6 formed in the matrix and on the aggregates surface indicates that its negative effect (inducing the castable expansion and allowing a more expressive slag infiltration [5]) in the AM-6CAC1S samples performance reduced the corrosion resistance of such material.

Although a higher amount of CA_6 is predicted to be formed after the first slag–AM-6CAC0S aggregates contact, the lower liquid content resulting from the slag–matrix interaction at the equilibrium state (Fig. 6a) seems to help inhibiting of the sample wearing, when compared to the silica containing composition.

The slag attack of the castable matrix will result in a higher liquid amount for the silica containing compositions after the

Table 4
Total amount of CA_2 and CA_6 phases predicted to be formed during the slag attack of the designed castables at 1500 °C.

Compositions	CA_2 (wt%)		CA_6 (wt%)	
	Matrix	Aggregates	Matrix	Aggregates
AM-6CAC0S	8.2	–	–	34.6
AM-6CAC1S	1.1	–	2.1	21.4
AM-6HA0S	–	–	10.9	–
AM-6HA1S	–	–	7.8	–

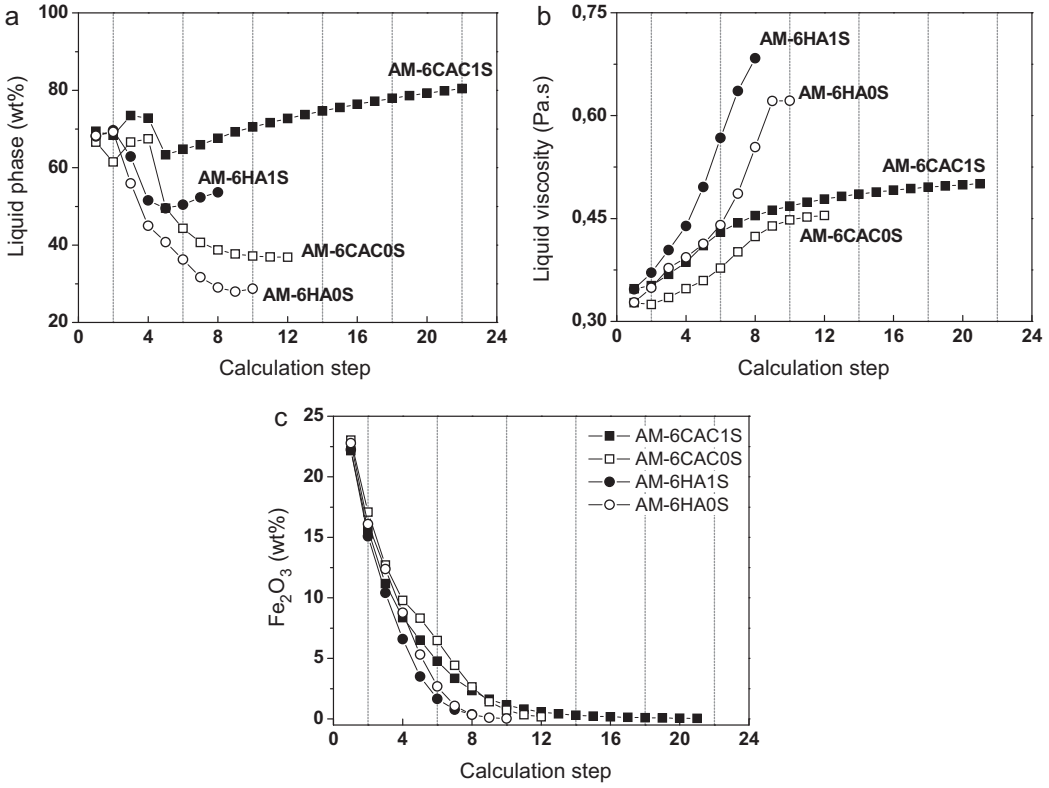

Fig. 6. Thermodynamic results for the slag–matrix interaction at 1500 °C. (a) Liquid content, (b) viscosity and its (c) Fe_2O_3 content.

final interaction steps (Fig. 6a) and the replacement of calcium aluminate cement by hydratable alumina should favor the corrosion resistance of the in situ spinel-containing refractories. Moreover, as expected, the addition of silica fume and the high alumina availability in the HA bonded compositions (followed by its dissolution into the liquid) can induce a slag viscosity increase (Fig. 6b). Considering the amount and viscosity of the liquid phase and the corrosion experimental results, it can be deduced that the lower slag penetration of the AM-6HA0S and AM-6HA1S is related to the higher slag viscosity attained after its reaction with the matrix components. Conversely, despite the higher liquid viscosity of the AM-6CAC1S (when compared with AM-6CAC0S), its higher content highlights the greater reactivity of this castable, which led to superior solid dissolution and slag penetration, as observed in Fig. 1.

A lower amount of Fe_2O_3 was attained in the resultant liquid (Fig. 6c) for the HA containing compositions, indicating that the higher spinel content (shown in Fig. 4) and its efficient role in trapping the Fe^{2+}, Fe^{3+} and Mn^{2+} ions from the molten slag helped increasing the slag viscosity and reducing the corrosion of AM-6HA0S and AM-6HA1S samples. Therefore, taking into account the liquid phase content and viscosity, the total amount of calcium hexaluminate and the number of calculation steps carried out for the slag–castable matrix simulation interaction, one will be able to attain a suitable estimative of the corrosion resistance behavior for the designed in situ spinel-containing castables (AM-6HA1S > AM-6HA0S > AM-6CAC0S > AM-6CAC1S) by applying the proposed thermodynamic model.

4. Conclusions

Based on the attained results, the binder source and the silica fume addition play a relevant role in the slag infiltration and corrosion resistance of in situ spinel-containing refractory castables. The cement-bonded samples presented higher slag infiltration and for non-silica fume containing castables, the CA_6 grains formed at the edges of the aggregates favored the precipitation of a dense CA_2 layer at the slag–matrix interface, suppressing further infiltrations. On the other hand, as CA_6 was only precipitated as acicular grains in the AM-6CAC1S matrix, the resulting higher porosity led to further slag infiltration and castable dissolution. Due to the CA_6 volumetric expansion and its expressive formation after the slag–matrix and slag–aggregates interactions (as predicted by the thermodynamic calculations), some aggregates fragmentation were identified in the AM-6CAC1S samples microstructure.

The castables containing hydratable alumina as a binder additive presented the highest corrosion resistance. The addition of silica fume to this system can result in a denser microstructure and, after the slag–matrix reactions, a more viscous slag can be attained. The presence of an alumina-rich spinel phase layer containing CA_2 grains close to the tabular alumina aggregates and at the slag–matrix interface reinforce the efficient role of the spinel phase in trapping ions from the slag, inhibiting the refractory wearing. Therefore, the calcium aluminate cement replacement for hydratable alumina as the binder source is a suitable alternative to improve the corrosion resistance of such castables.

Based on the number of calculation steps carried out for the slag–castable matrix simulation interaction, liquid phase content and viscosity, and the total amount of calcium hexaluminate phase, the thermodynamic calculations matched to the experimental observations and the following corrosion resistance ranking was attained: AM-6HA1S > AM-6HA0S > AM-6CAC0S > AM-6CAC1S. Thus, the improved simulation model applied in this work proved to be an efficient tool for the evaluation of the in situ spinel-containing refractory castables corrosion behavior.

Acknowledgments

The authors are grateful to the Federation for International Refractory Research and Education (FIRE), Magnesita Refratários S.A. (Brazil), FAPESP and CNPq. Additionally, the authors are thankful to G.G. Morbioli for the castables processing.

References

[1] S. Mukhopadhyay, P.K. Das Poddar, Effect of preformed and in situ spinels on microstructure and properties of a low cement refractory castable, Ceram. Int. 30 (2004) 369–380.
[2] P. Korgul, D.R. Wilson, W.E. Lee, Microstructural analysis of corroded alumina–spinel castable refractories, J. Eur. Ceram. Soc. 17 (1997) 77–84.
[3] L.A. Díaz, R. Torrecillas, A.H. de Aza, P. Pena, Effect of spinel on slag attack resistance of high alumina refractory castables, J. Eur. Ceram. Soc. 27 (2007) 4625–4631.
[4] H. Sarpoolaky, S. Zhang, B.B. Argent, W.E. Lee, Influence of grain phase on slag corrosion of low-cement castable refractories, J. Am. Ceram. Soc. 84 (2) (2001) 426–434.
[5] M.A.L. Braulio, A.G. Tomba Martinez, A.P. Luz, C. Liebske, V.C. Pandolfelli, Basic slag attack of spinel-containing refractory castables, Ceram. Int. 37 (2011) 1935–1945.
[6] M.A.L. Braulio, L.R.M. Bittencourt, V.C. Pandolfelli, Magnesia grain size effect on in situ spinel refractory castables, J. Eur. Ceram. Soc. 28 (15) (2008) 2845–2852.
[7] K. Jono, J. Mori, Y. Toritani, Effect of alumina grain size on spinel formation, Taikabutsu Overseas 16 (1996) 12–16.
[8] M.A.L. Braulio, L.R.M. Bittencourt, V.C. Pandolfelli, Selection of binders for in situ spinel refractory castables, J. Eur. Ceram. Soc. 29 (2009) 2727–2735.
[9] R. Salomão, V.C. Pandolfelli, The role of hydraulic binders on magnesia containing refractory castables: calcium aluminate cement and hydratable alumina, Ceram. Int. 35 (2009) 3117–3124.
[10] M. Furher, A. Hey, W.E. Lee, Microstructural evolution in self-forming spinel/calcium aluminate castable refractories, J. Eur. Ceram. Soc. 18 (1998) 813–820.
[11] E.Y. Sako, M.A.L. Braulio, D.H. Milanez, P.O. Brant, V.C. Pandolfelli, Microsilica role in the CA_6 formation in cement-bonded spinel refractory castables, J. Mater. Process. Technol. 209 (2009) 5552–5557.
[12] M.A.L. Braulio, L.R.M. Bittencourt, V.C. Pandolfelli, Microsilica road-map for alumina magnesia castables expansion, Refract. Appl. News 15 (2010) 12–15.
[13] M.A.L. Braulio, P.O.C. Brant, L.R.M. Bittencourt, V.C. Pandolfelli, Microsilica or MgO grain size: which one mostly affects the in situ spinel refractory castable expansion? Ceram. Int. 35 (2009) 3327–3334.
[14] M.A.L. Braulio, D.H. Milanez, E.Y. Sako, L.R.M. Bittencourt, V.C. Pandolfelli, Are refractory aggregates inert? Am. Ceram. Soc. Bull. 87 (2008) 27–31.
[15] A.P. Luz, M.A.L. Braulio, A.G. Tomba Martinez, V.C. Pandolfelli, Thermodynamic simulation models for predicting Al_2O_3–MgO castable chemical corrosion, Ceram. Int. (2011), doi:10.1016/j.ceramint.2011.05.049.
[16] R.G. Pileggi, A.R. Studart, M.D.M. Innocentini, V.C. Pandolfelli, High performance refractory castables, Am. Ceram. Soc. Bull. 81 (2002) 37–42.
[17] B.A. Vázquez, A. Caballero, P. Pena, Quaternary system Al_2O_3–CaO–MgO–SiO_2. II. Study of the crystallisation volume of $MgAl_2O_4$, J. Am. Ceram. Soc. 88 (2005) 1949–1957.
[18] G.J. Browning, G.W. Bryant, H.J. Hurst, J.A. Lucas, T.F. Wall, An empirical method for the prediction of coal ash slag viscosity, Energy Fuels 17 (3) (2003) 731–737.
[19] B. Myhre, B. Sandberg, A.M. Hundere, Castables with MgO–SiO_2–Al_2O_3, in: Proceedings of XXVI ALAFAR Congress, San Juan, Puerto Rico, (1997), pp. 10–14.
[20] K. Goto, B.B. Argent, W.E. Lee, Corrosion of MgO–$MgAl_2O_4$ spinel refractory bricks by calcium aluminosilicate slag, J. Am. Ceram. Soc. 80 (2) (1997) 461–471.
[21] J.P. Guha, Reaction chemistry in dissolution of polycrystalline alumina in lime–alumina–silica slag, Br. Ceram. Trans. 96 (6) (1997) 231–236.